Electrochimica Acta 96 (2013) 243–252

Contents lists available at SciVerse ScienceDirect

Electrochimica Acta

journal homepage: www.elsevier.com/locate/electacta

PtSnNi/C nanoparticle electrocatalysts for the ethanol oxidation reaction: Ni stability study

Luanna Silveira Parreira[a], Júlio César Martins da Silva[a], Melina D'Villa -Silva[a], Fernando Carmona Simões[a], Samara Garcia[a], Ivanise Gaubeur[a], Marco Aurélio Liutheviciene Cordeiro[b], Edson Roberto Leite[b], Mauro Coelho dos Santos[a,*]

[a] Laboratório de Eletroquímica e Materiais Nanoestruturados – CCNH – Centro de Ciências Naturais e Humanas, Universidade Federal do ABC, CEP 09.210-170, Rua Santa Adélia 166, Santo André, SP, Brazil
[b] Departamento de Química, Universidade Federal de São Carlos, CEP 13.565-905, Rodovia ashington Luís km 235, São Carlos, SP, Brazil

ARTICLE INFO

Article history:
Received 13 September 2012
Received in revised form 6 February 2013
Accepted 8 February 2013
Available online 16 February 2013

Keywords:
Ethanol oxidation
PtSnNi/C electrocatalysts
Accelerated stress tests

ABSTRACT

This work describes the use of Pt_3Sn/C, Pt_3Ni/C and Pt_3SnNi/C nanoparticle electrocatalysts with a 20% metal loading on carbon prepared using the polymeric precursor method for the ethanol oxidation reaction (EOR). XRD measurements revealed the presence of segregated Pt and NiO phases in the Pt_3Ni/C electrocatalysts, whereas for Pt_3SnNi/C, there was some evidence that Ni and Sn atoms are incorporated into the Pt structure with the presence of segregated SnO_2 and NiO phases. The mean crystallite sizes were 3.6, 5.7 and 7.2 nm for Pt_3Sn/C, Pt_3Ni/C, and Pt_3SnNi/C, respectively. The onset oxidation potential obtained for the EOR using Pt_3SnNi/C was close to 0.22 V. Chronoamperometric measurements revealed that the highest current densities for the EOR were obtained using the Pt_3SnNi/C nanoparticle electrocatalysts (16 mA mg_{Pt}^{-1}). Based on the Ni accelerated stress tests, this element was more stable in the ternary material. In contrast, there was a change in the product formation pathways before (acetaldehyde and acetic acid were the primary products) and after the accelerated stress tests (acetaldehyde was the primary product) for the Pt_3SnNi/C catalyst. The experimental results indicate that the Pt_3SnNi/C electrocatalysts exhibited better electrocatalytic activity compared to the other electrocatalysts for the EOR. It is suggested that this activity is related to the presence of Ni, which can modify the electronic structure of Pt and combine with Sn to facilitate the removal of adsorbed CO on the surface of the Pt, thereby promoting the EOR.

1. Introduction

Ethanol is a renewable resource derived from biomass [1] (which absorbs a considerable amount of CO_2 that is released into the atmosphere), and it is considered to be a neutral product for the production of carbon dioxide and consequently of greenhouse gases.

Ethanol is easy to transport and store and is less toxic and has a higher energy density (8.01 kWh kg^{-1} vs 9.63 kWh kg^{-1}) than methanol, which makes it attractive for use in low-temperature fuel cells [2,3]. Although DEFCs have a lower theoretical potential (1.15 V vs. 1.23 V for H_2-fuel cells under standard conditions), their theoretical thermodynamic efficiency of 97% is higher than that of H_2-fuel cells (83%) [4]. However, the electrochemical oxidation of ethanol [5,6] is complex because 12 electrons must be released to cleave the C–C bond [7]. During the ethanol oxidation reaction, adsorbed CO (carbon monoxide) is produced while CH_3CHO (acetaldehyde), CH_3COOH (acetic acid) and CO_2 (carbon dioxide) are the main products. In addition, two carbon atom products can also be detected. The formation of acetaldehyde and acetic acid can reduce the fuel cell efficiency because the 12 electrons are not released [8].

Sn has been shown to exhibit good activity as an auxiliary metal for Pt-based electrocatalysts in the ethanol oxidation reaction [9–11]. PtSn can be obtained as alloys and/or in a non-alloyed oxidized state depending on the preparation method [12–14]. The activity of Pt/Sn is strongly related to the degree of PtSn alloying and the ethanol oxidation reaction mechanism [15,16]. Non-alloyed PtSn can offer OH species at lower potentials than Pt, and the CO-like intermediate strongly adsorbed onto the Pt surface reacts with the OH species and the Pt active sites are released [17]. However, during the formation of the alloy, the valence electrons of the Sn atoms can be transferred to neighboring Pt atoms, which modifies the unfilled d band states of the Pt [18]. This modification may cause

* Corresponding author. Tel.: +55 11 4996 0163; fax: +55 11 4996 0090.
E-mail address: mauro.santos@ufabc.edu.br (M.C. dos Santos).

0013-4686/$ – see front matter © 2013 Elsevier Ltd. All rights reserved.
http://dx.doi.org/10.1016/j.electacta.2013.02.054

a weaker bond between the Pt—CO intermediate on the surface [19–21], which decreases CO poisoning and improves the intermediate oxidation to CO_2 by oxygen-containing species on the Sn surface [22].

Souza et al. [23] suggested that the good performance of a direct ethanol fuel cell using the Pt_3Sn/C electrocatalyst as an anode is due to the presence of the Pt_3Sn alloy phase through an electronic effect. In contrast, Jiang et al. [24] have shown that the oxidation state of Sn is the determining factor for the influence of Sn on Pt. In addition, the stability of the electrode, which is dependent on the electrocatalyst preparation method [21], is increased for high oxidation states of tin and promotes the electrochemical oxidation of ethanol.

Nickel [4,25] can also be used as an auxiliary metal with Pt in the electrocatalysts for the oxidation of ethanol. Huber et al. [26] suggested that the presence of nickel oxides modifies the electronic properties of Pt for the oxidation of ethanol, and its effect is explained by both electronic effects and a bifunctional mechanism. As observed for other oxides, the formation of the NiO_x electrocatalyst may provide hydroxyl species that aid in the oxidative removal of CO at lower potentials compared to Pt, which releases their active sites (bifunctional mechanism). PtNi alloying changes the network parameters and reduces the d band center of the Pt, which weakens the adsorption of CO and reduces poisoning of Pt sites. The PtNi alloying also weakens the adsorption of small organic molecules, such as ethanol, that can decrease the efficiency of the electrocatalyst. This effect is also observed with the addition of metals such as Sn [22]. Furthermore, the addition of Ni also disfavors the adsorption of hydroxyl species, and this feature facilitates the use of Ni in the electrocatalysis of the oxygen reduction reaction [27]. However, nickel in the presence of Sn may facilitate cleavage of the C—C bond and promote desorption of the CO that is adsorbed on the Pt surface through a "water–gas" exchange reaction [26], which increases the selectivity for hydrogen production.

In addition to the binary alloys, ternary alloys [28–30] are also being developed for oxidizing intermediate species on Pt surfaces during the ethanol oxidation reaction, which reduces poisoning of the catalyst. However, the function of the third metal has not been fully elucidated.

Almeida et al. [31] observed that the addition of Ni on both Pt/C and PtSn/C catalysts significantly shifted the onset potential for the oxidation of both ethanol and CO toward lower potentials, thereby enhancing the catalytic activity, especially for the ternary PtSnNi/C composition. Bonesi and coworkers [32] performed the electrooxidation of ethanol on carbon-supported Pt–Ru–Ni and Pt–Sn–Ni catalysts that were prepared using the ethylene glycol-reduction process. These catalysts were electrochemically studied using cyclic voltammetry measurements at 50 °C in direct ethanol fuel cells. The addition of nickel to the anode improved the performance of the DEFC. This improvement in performance was most likely due to the presence of some PtSn alloys or tin oxide and to the nickel oxide species that favor the oxidation of absorbed CO-like species. Ribadeneira and Hoyos [33] prepared the binary electrocatalysts PtSn/C and PtRu/C and reported that the introduction of Ni contributes to an increase in the electrocatalytic activity of the materials for the ethanol oxidation reaction.

One of the most important factors in the application of proton exchange membrane fuel cells is the lifetime of the device. In this context, the durability of the catalyst layer is the primary challenge, and this topic is currently receiving considerable research attention. Accelerated stress tests [34] have seen increased use primarily due to the reduced time required for experiments to evaluate the lifetime degradation. In addition, the analysis can be conducted using an electrochemical half-cell (*ex situ*) system.

Zignani et al. [35] prepared carbon-supported Pt and Pt–Ni (1:1) nanoparticles through the reduction of metal precursors with $NaBH_4$ and evaluated their activity for the oxygen reduction reaction. The stability of the electrocatalysts was examined using tests that involved repetitive potential cycling (1000 cycles) between 0.5 and 1.0 V vs. RHE at 20 mV s^{-1}. After 1000 cycles, a complete loss of the non-alloyed and part of the alloyed Ni was observed for the Pt–Ni/C catalyst following the repetitive potential cycling. The ORR activity of Pt–Ni/C was less than that of both the as-prepared Pt–Ni/C and the cycled Pt/C. This result was explained in terms of the surface enrichment of Pt and an increase in the crystallite size of the Pt–Ni/C catalyst.

The aim of this work is to study the influence of Sn and Ni as auxiliary metals in Pt-based nanoparticle electrocatalysts during the catalytic oxidation of ethanol. In addition, determining the stability of the electrocatalysts containing Ni during accelerated stress tests is also a primary goal. Therefore, Pt_3Sn/C, Pt_3Ni/C and Pt_3SnNi/C nanoparticles with a metal loading of 20% by weight on a carbon support were prepared using the polymeric precursor method. The crystalline phases and the mean crystallite and particle sizes were determined using XRD and TEM. Electrochemical techniques, such as cyclic voltammetry and chronoamperometry, were used to evaluate the electrocatalytic activity of the materials for the oxidation of ethanol. The reaction pathways for the oxidation of ethanol were analyzed using the *in situ* FTIR-ATR technique both before and after the Ni accelerated stress tests. The dissolution of nickel during the accelerated stress tests was evaluated using graphite furnace atomic absorption spectrometry (GF AAS).

2. Materials and methods

2.1. Preparation of the electrocatalysts

The nanoparticle electrocatalysts were prepared using the polymeric precursor method developed by Souza et al. [23]. The precursor resin was formed by dissolving citric acid with ethylene glycol at 60 °C, followed by the addition of the metal solution (H_2PtCl_6, $SnCl_2$ and $NiCl_2$ from Aldrich). In this case, the metal/citric acid/ethylene glycol molar ratio was 1:50:400. The resin was added to the high surface area carbon Vulcan XC-72R to obtain catalysts with a metal loading of 20% (w/w) on carbon. After this step, the mixture was homogenized in an ultrasonic bath and thermally treated under a N_2 atmosphere for 2 h at 400 °C. A suspension of Milli-Q water, Nafion® and the electrocatalyst was homogenized in an ultrasonic bath and applied to the glassy carbon electrode for the electrochemical analyses.

2.2. Physical characterization

The electrocatalysts were physically characterized using X-ray diffraction (XRD) with a Bruker Focus diffractometer with a CuKα radiation source operating in the continuous scan mode (2° min^{-1}) from 20 to 80° 2θ to determine the crystalline phases and to estimate the mean crystallite sizes.

Transmission electron microscopy (TEM) analyses were performed using a high resolution Joel microscope operating at 300 kV to observe the morphology and to measure the particle sizes. All of the samples for the TEM analyses were prepared by ultrasonically dispersing the catalyst particles in a formaldehyde solution. Drops of the suspension were deposited onto a standard Cu grid and covered with a carbon film. The average particle size was determined using the Image J software package, and more than 150 different particles were analyzed.

2.3. Electrochemical characterization and activities of the nanoparticle electrocatalysts

Electrochemical experiments were performed using an Autolab model PGSTAT 302 N potentiostat/galvanostat to examine the

behavior of the electrocatalysts in a 1.0 mol L^{-1} solution of ethanol and a 0.5 mol L^{-1} solution of H_2SO_4. The measurements were performed at 25 °C in a deoxygenated medium by purging the electrolyte with nitrogen for 10 min prior to each measurement.

Cyclic voltammograms were recorded using a scan rate of 50 mV s^{-1} (in 0.5 mol L^{-1} H_2SO_4) and 10 mV s^{-1} (in 1.0 mol L^{-1} ethanol) in the potential range from 0.2 to 0.9 V versus the reversible hydrogen electrode (RHE). A three-electrode cell was used to perform the analyses, and platinum was used as the counter electrode and RHE as the reference electrode. The working electrode was a glassy carbon disc with an exposed area of 0.16 cm^2 that was recovered from the dispersion prepared with the electrocatalyst. Chronoamperometry measurements were performed at 0.5 V for 1800 s in a 1.0 mol L^{-1} ethanol solution.

For the CO stripping measurements, a 0.5 mol L^{-1} H_2SO_4 solution was used as an electrolyte. Subsequently, CO was adsorbed at 20 mV for 15 min under stirring. After removal of the CO (N_2 purge for >30 min), the electrocatalyst was subjected to three consecutive voltammetric cycles at a scan rate of 10 mV s^{-1} in the potential range of 0.05–1 V versus the reversible hydrogen electrode (RHE). As a control, the profile of the voltammogram obtained after the oxidation of CO was compared to the voltammogram recorded under similar conditions prior to the adsorption of CO.

The electrocatalysts were submitted to accelerated stress tests by repetitive potential cycling (1000 cycles) between 0.05 and 1.0 V vs. RHE at 50 mV s^{-1}. After the stress test, the solution was analyzed by GF AAS to quantify the dissolution of Ni, and the electrocatalysts were retested for the ethanol oxidation reaction.

For monitoring the formation of intermediate species and final products during the ethanol electrochemical oxidation reaction, the *in situ* ATR-FTIR infrared spectroscopy method adapted from the work of Silva et al. was used [15]. This measurement was performed using a Varian® IR 660 spectrometer that was equipped with a MCT detector cooled with liquid N_2 and an ATR (attenuated total reflectance) crystal plate accessory with a diamond/ZnSe. The experiments were performed at 25 °C. The 1 mol L^{-1} ethanol solution was used in a 0.1 mol L^{-1} $HClO_4$ medium. After the experiment, all of the adsorption bands were deconvoluted into Lorentzian line forms. Therefore, the intensity and line width of each band could be analyzed individually. In this work, the integrated intensities of the acetic acid, acetaldehyde and CO_2 bands are presented.

2.4. Analysis of metal dissolution

The GF AAS measurements were performed using a Zeenit 600 (Analytik Jena AG, Jena, Germany) equipped with a hollow nickel cathode lamp (operated at 4.0 mA, with a spectral bandpass of 0.8 nm and wavelength of 232.00 nm), a transversely heated graphite tube atomizer and a Zeeman background corrector. Argon (99.998% (v/v)) was used as the purge gas. All of the measurements were performed using the integrated absorbance (peak area) and conducted in triplicate.

Aliquots containing 10 μL of the sample were added to the graphite platform. The pyrolysis and atomization temperatures were investigated in the ranges of 1000–1800 °C and 2000–2600 °C, respectively. Both studies were performed in the presence and absence of the chemical modifier (5 μg Pd + 2.5 μg Mg). The peak shapes, background absorption and relative standard deviation were considered for selecting the proper furnace conditions [36].

In the presence of the Pd + Mg chemical modifiers, the pyrolysis and atomization temperatures were 1400 °C and 2400 °C, respectively. The optimized temperature program for the determination of Ni is presented in Table 1.

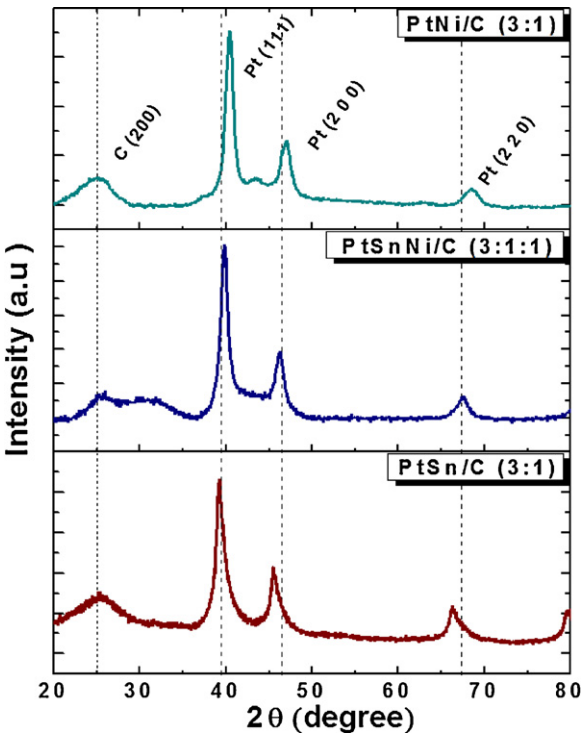

Fig. 1. X-ray diffraction patterns of the PtSn/C (3:1), PtNi/C (3:1) and PtSnNi/C (3:1:1) electrocatalysts prepared using the polymeric precursor method.

3. Results and discussion

3.1. Physical characterization

Fig. 1 presents the X-ray diffraction pattern of the as-prepared carbon-supported PtSn/C (3:1), PtNi/C (3:1) and PtSnNi/C (3:1:1) electrocatalysts. The diffraction peak at $2\theta = 25°$ is associated with the amorphous phase of carbon Vulcan XC-72. All of the X-ray diffraction patterns present three reflections that correspond to the (1 1 1), (2 0 0) and (2 2 0) planes that are characteristic of the face-centered cubic structure of Pt.

For the Pt_3Ni/C electrocatalysts, the 2θ angles of the peaks are shifted to higher values, which indicate the presence of a crystal lattice contraction. In other words, there is a small decrease in the lattice parameter of the Pt/C structure (3.876 Å). Nearly 40% of the electrocatalyst is composed of an alloy containing Pt and Ni (Pt_3Ni), as calculated using a Nelson–Riley plot [23,35]. It was also possible to observe the presence NiO at $2\theta \approx 43°$ [37]. Park et al. [38] observed the presence of Pt/Ni alloys (with metallic nickel in the platinum lattice) and amorphous Ni oxides (such as NiO, Ni–$OH)_2$, and NiOOH) in the PtNi electrocatalysts through XRD measurements, which was then confirmed by XPS. However, the addition of Sn shifted the 2θ angles to lower values and promoted expansion of the crystal lattice due to the increase in the lattice parameter. For the ternary electrocatalyst PtSnNi/C (3:1:1), both Sn and Ni are present and cause opposite effects, which explains the very similar lattice parameter values between the ternary electrocatalyst and pure Pt/C [35,39]. In this work, the peaks at approximately $2\theta = 34°$ and 52° are consistent with the cassiterite phase of SnO_2, which was observed in both PtSnNi/C and PtSn/C [40]. However, the presence of amorphous NiO cannot be disregarded [35] in the PtSnNi/C nanoparticle electrocatalysts. The average crystallite sizes estimated using the Debye–Scherrer equation and the lattice parameters for all of the electrocatalysts are presented in Table 2.

Fig. 2a and c presents the transmission electron microscopy (TEM) images of the carbon-supported PtNi (3:1) and PtSnNi (3:1:1)

Table 1
Graphite furnace temperature program for the determination of Ni in samples.

Stage	Temperature (°C)	Ramp (°C s^{-1})	Hold (s)	Ar flow rate (L min^{-1})
Drying	100	5	10	1.0
Pyrolysis	1400	100	10	1.0
Atomization	2400	1100	10	0
Cleaning	2600	100	3	1.0

Table 2
Structural parameters of the PtSn/C, PtNi/C and PtSnNi/C nanoparticle electrocatalysts determined from the Pt (2 2 0) peak.

Electrocatalyst	Lattice parameter (Å)	Crystallite size (nm)
PtSn/C (3:1)	3.984	4.92
PtNi/C (3:1)	3.856	3.72
PtSnNi/C (3:1:1)	3.912	5.14

nano-electrocatalysts and their corresponding particle size distribution histograms based on the observation of more than 100 nanoparticles, which are presented in Fig. 2b and d. The distribution of metal nanoparticles on the Vulcan XC-72 carbon is heterogeneous with some agglomerates over the carbon particles (primarily for the PtNi/C electrocatalyst) where small islands are formed by Pt and Ni. However, PtSnNi/C exhibits well-dispersed nanoparticles on the surface of the support that contributes to its catalytic activity (further discussion is presented below).

The two electrocatalysts have crystalline structures, as indicated by the clear lattice fringes in the high resolution TEM images (the insets in Fig. 2a and b). The measured lattice fringe distance differs from the value measured (0.214 nm) for the PtNi alloy particles [27], which is most likely due to the presence of NiO in the matrix. The average particle size is 4.98 nm with a standard deviation of 1.72 nm for PtNi/C and 3.72 nm (particle size) with a standard deviation of 1.06 nm for PtSnNi/C. These data are consistent with the results from the X-ray diffraction measurements.

3.2. Electrochemical characterization and activities of the electrocatalysts

The electrocatalytic activities of the prepared materials were evaluated for the oxidation of ethanol (Fig. 3). The onset potential for the oxidation of ethanol on PtSnNi/C (3:1:1) was 0.22 V, which is similar to the value obtained using Pt_3Sn/C (0.21 V) and less than that obtained using the PtNi/C (3:1) (0.57 V) and PtSn/C E-Tek (0.40 V) electrocatalysts. The maximum current densities for the oxidation of ethanol were 736 mAmg_{Pt}^{-1}, 267 mAmg_{Pt}^{-1}, 4 mAmg_{Pt}^{-1} and 153 mAmg_{Pt}^{-1} for the PtSnNi/C (3:1:1), Pt_3Sn/C, PtNi/C (3:1) and PtSn/C E-Tek electrocatalysts, respectively. In addition, two peaks for the ethanol oxidation were observed during the forward scan [41,42]. The first peak (at 0.6 V) corresponds to

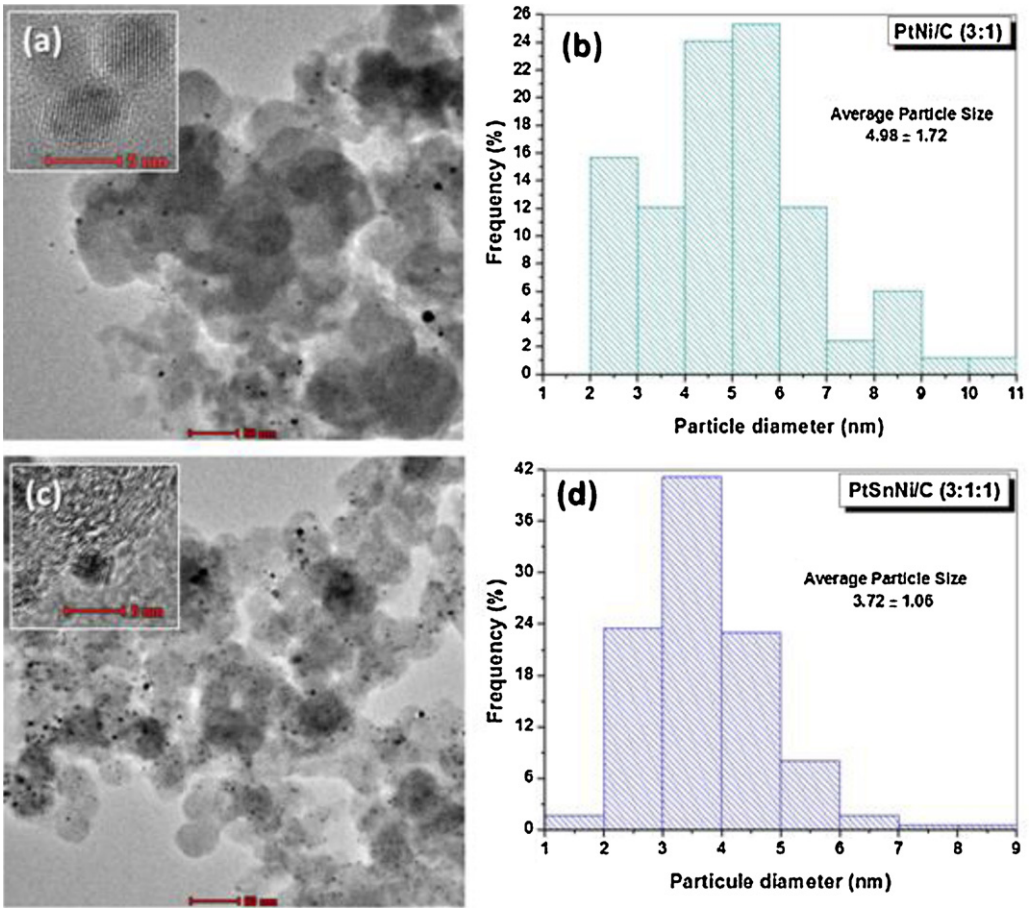

Fig. 2. (a) Transmission electron microscopy image of PtNi/C (3:1) with a high resolution image inset; (b) size-distribution histogram of PtNi/C (3:1); (c) Transmission electron microscopy image of PtSnNi/C (3:1:1) with a high resolution image inset; (d) size-distribution histogram of PtSnNi/C (3:1:1).

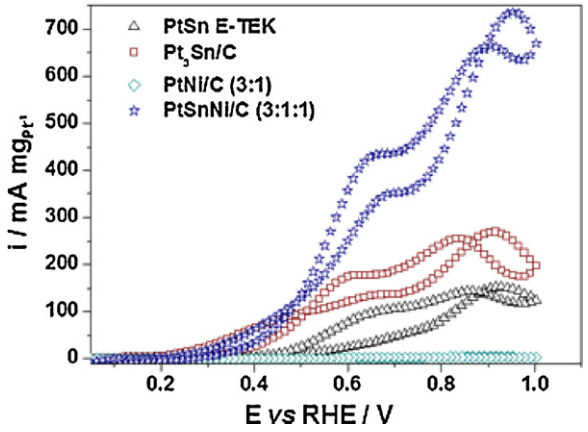

Fig. 3. Cyclic voltammograms of the PtSn/C (3:1), PtNi/C (3:1) and PtSnNi/C (3:1:1) nano-electrocatalysts prepared using the polymeric precursor method and the Pt/C E-Tek commercial electrocatalystobtained at a scan rate of 10 mV s^{-1} in a 1 mol L^{-1} CH_3CH_2OH + 0.5 mol L^{-1} H_2SO_4 solution.

the oxidation of ethanol to CO_2, and the second peak (at 0.9 V) is related to the formation of acetaldehyde and acetic acid. Simões et al. [7] studied the electrooxidation of ethanol and found that the first peak appears at a potential where surface-bound OH is formed on Pt, whereas the second oxidation peak depends on the Sn content and is located on the remaining Pt–H sites (i.e., after desorption of the oxide species from the electrode surface).

The binary PtNi/C (3:1) electrocatalyst exhibited both segregated Ni oxide and Pt_3Ni phases. The presence of Ni decreases the Pt d-band center, weakening the adsorption of the hydroxyl species, which improves the O_2 reduction activity on the Pt-coated Pt_3Ni surfaces [43] and decreases the ethanol oxidation reaction, as shown by the cyclic voltammogram results (see Fig. 3) with the highest onset potential for ethanol oxidation. However, Ni can be

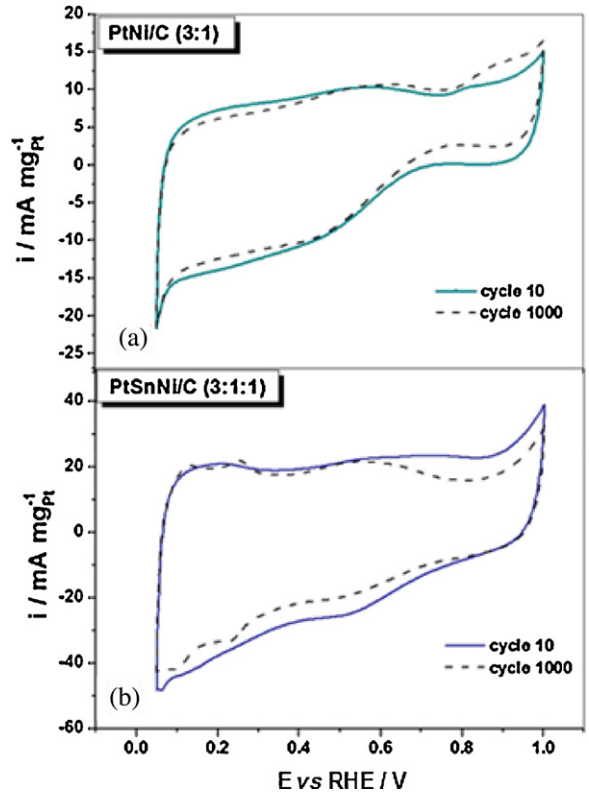

Fig. 4. Cyclic voltammograms of (a) PtNi/C (3:1) and (b) PtSnNi/C (3:1:1) nano-electrocatalysts prepared using the polymeric precursor method before and after the accelerated stress tests. The voltammograms were recorded at a scan rate of 10 mV s^{-1} in a 0.5 mol L^{-1} H_2SO_4 solution.

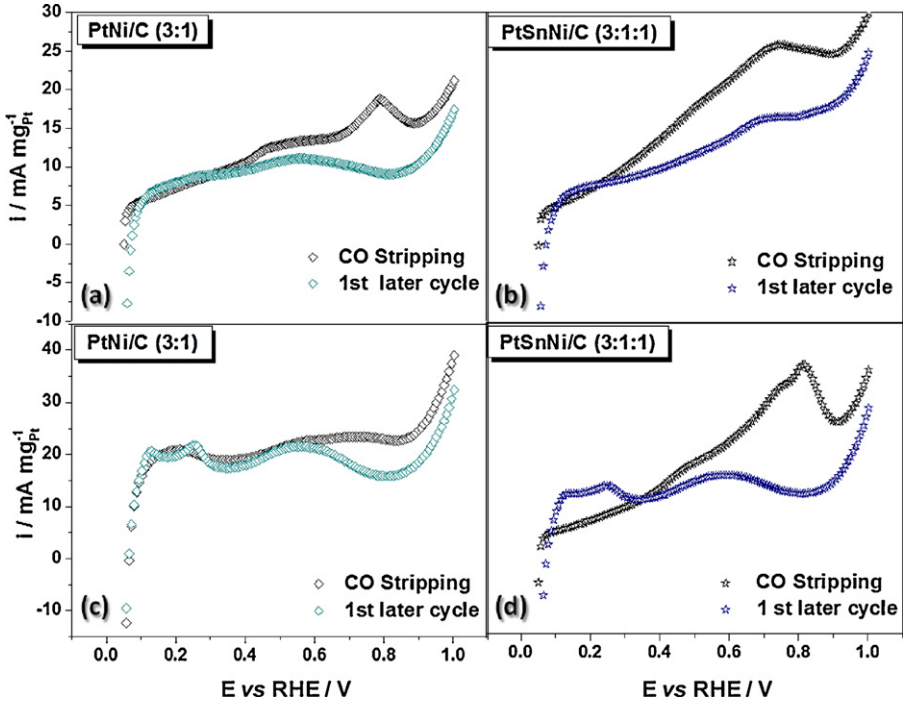

Fig. 5. CO-stripping voltammograms for (a) PtNi/C (3:1) and (b) PtSnNi/C (3:1:1) before the accelerated stress tests; (c) PtNi/C (3:1) and (d) PtSnNi/C (3:1:1) after the accelerated stress tests in an electrolyte containing 0.5 mol L^{-1} H_2SO_4. The scanning rate was 50 mV s^{-1}. T = 25 °C.

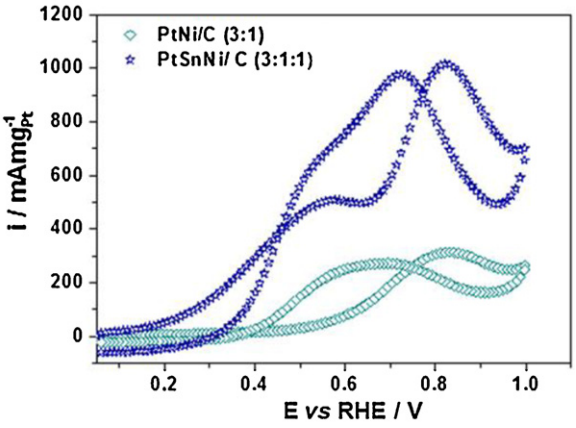

Fig. 6. Cyclic voltammogramsfor the EOR using PtNi/C (3:1) and PtSnNi/C (3:1:1) nano-electrocatalysts prepared using the polymeric precursor method after the accelerated stress tests in 1 mol L^{-1} CH_3CH_2OH + 0.5 mol L^{-1} H_2SO_4 at a scan rate of 10 mV s^{-1}.

removed from the electrode surface at a potential greater than 1 V in acidic media [44], which decreases the activity and stability of the electrocatalyst for the ethanol oxidation reaction.

To examine the stability of Ni in the electrocatalysts, electrochemical accelerated stress tests were performed. After 1000 voltammetric cycles (from 0.05 to 1.0 V), the profiles shown in Fig. 4 were obtained, and the nickel that was present in the solution after the tests was measured using a GFAAS.

A change in the voltammetric profile of both electrocatalysts was observed. For the PtNi/C (3:1) electrocatalyst, there was an increase in the oxidation peak of Ni at 0.9 V [43], which was not present before. This increase is due to the Ni atom being 11% smaller in size than Pt and to the formation of an interstitial solid solution [45], which becomes exposed during the voltammetric cycles undergoing dissolution. Note that if the surfaces of the Pt nanoparticles are covered by Ni or its oxides/hydroxides, a lower catalytic activity may result [43], which is related to both Pt unexposed sites and the inhibition of hydrogen UPD adsorption and desorption, as shown in Fig. 4a.

For PtSnNi/C (Fig. 4b), the observed capacitive profile may be related to the presence of Ni and Sn oxide/hydroxide species on the surface, which increases the voltammetric charge [33]. However, after cycling, these species are most likely reduced, exposing the Pt sites (hydrogen adsorption and desorption between 0.05 and 0.4 V), as observed for that region. There are no oxidation processes associated with Ni, which was previously shown using PtNi/C. The surface layer of the electrocatalysts may contain Ni hydroxides, $Ni(OH)_2$ and NiOOH, which are relatively stable in acidic media [46]. This stability was evaluated by the dissolution process using GFAAS, where the Ni in the binary electrocatalyst (percentage of dissolved Ni was 1.9%) exhibited a dissolution that was 6.5-times greater than the ternary one (percentage of dissolved Ni was 0.3%). Therefore, the presence of a process related to Ni dissolution is clearly observed for PtNi/C, as shown in Fig. 4a. In addition, the presence of Sn may be responsible for the high Ni stability in the electrocatalyst [47]. In electrocatalysts containing Ni, it may be present in the form of hydroxides that exhibit satisfactory stability in acidic media, which have been observed using XPS in other studies [44,45,48]. In addition, the formation of an interstitial solid solution [7] with Pt may help stabilize the Ni, which is further improved by the presence of Sn. These metals can form a solid solution that has greater resistance to corrosion in acidic media [49,50]. Therefore, the migration of nickel to the solution is not easy, which was observed during the GFAAS analysis.

The changes in the structure of the electrocatalyst during the accelerated stress tests influence their electrocatalytic activity. Therefore, the adsorption of CO and the oxidation of ethanol were examined both before and after the tests.

The strongly adsorbed CO tolerance on the Pt-based electrocatalyst surfaces is an important factor in the ethanol oxidation reaction. The CO stripping voltammetry results are shown in Fig. 5. Before the stress tests, the lowest onset potential and the highest current density for the oxidation of CO were obtained using the PtSnNi/C electrocatalyst. In general, CO is adsorbed on the Pt surface in a bridge configuration in regions of low potentials [21]. The presence of Sn [51] and Ni [43] can weaken the strength of the adsorption of CO through electronic effects, which changes the CO adsorption mode. In addition, the dissociation of water can provide $(OH)_{ads}$ and remove the intermediate products from the surface of the electrocatalyst via a bifunctional mechanism [52]. Therefore, the CO oxidation current density is reflective of the ability of the electrocatalyst to form oxyhydroxide species for the oxidation of CO. Because the transfer ratio of $(OH)_{ads}$ is accelerated, i.e., there are more available OH_{ads} sites, the oxidation rate for CO-like intermediates at the surface is promoted, which increases the activity for the oxidation of ethanol and the tolerance of the electrocatalyst for CO [26].

For both Pt-based electrocatalysts, the oxidation of CO after the stress test begins at higher onset potentials with higher current peak densities than those before the stress tests. This result can be explained by a reduction in the oxyhydroxide species that are reduced during the tests in addition to the exposure of Pt sites that have a high adsorption strength for CO with high cur-

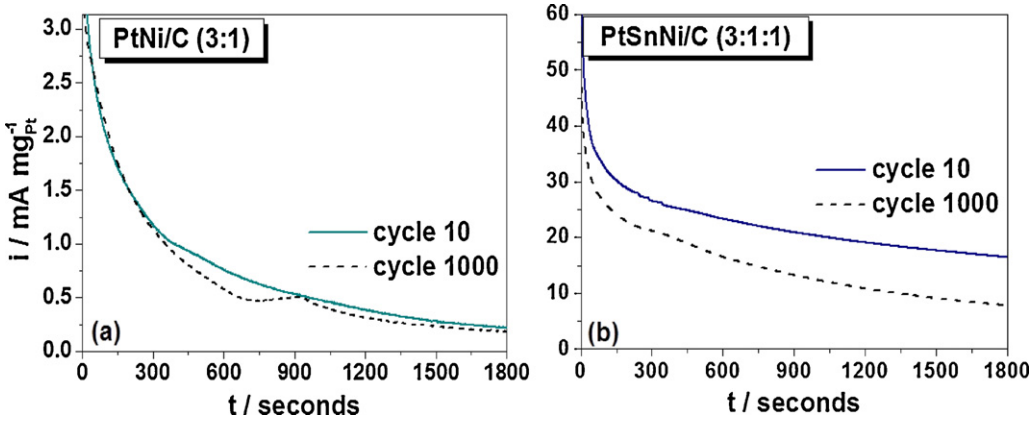

Fig. 7. Chronoamperometric curves for the EOR using (a) PtNi/C (3:1) and (c) PtSnNi/C (3:1:1) nano-electrocatalysts prepared using the polymeric precursor method before and after the accelerated stress tests in 1 mol L^{-1} CH_3CH_2OH + 0.5 mol L^{-1} H_2SO_4 at an applied potential of 0.5 V for 1800 s.

rent densities for the oxidation of CO [53]. In fact, these results are in agreement with those obtained using voltammetry stress tests, which are presented in Fig. 4a and b for both Pt-based electrocatalysts.

The catalytic activity and stability of the PtSnNi/C and PtNi/C electrocatalysts for the oxidation of ethanol were investigated using cyclic voltammetry (Fig. 6) and chronoamperometric measurements (Fig. 7) before and after the accelerated stress tests. The onset potential for the oxidation of ethanol on PtSnNi/C (3:1:1) was 0.23 V, which is similar to the value obtained prior to the stress test (0.22 V). Additionally, using PtNi/C (3:1) after stress test was observed the onset potential close to presented before stress test (0.57 and 0.58, respectively). In addition, the maximum current densities for the oxidation of ethanol were 821 $mAmg_{Pt}^{-1}$ and 326 $mAmg_{Pt}^{-1}$ for the PtSnNi/C (3:1:1) and PtNi/C (3:1) electrocatalysts, respectively.

The slight shift in the oxidation onset potential may be related to the chemical stability of the electrocatalyst due to a low dissolution of Ni and an increase in the current peak density due to the oxidation of intermediates formed during the process. In the chronoamperometric measurements (Fig. 7) at 0.5 V, the current density for the EOR using the PtSnNi/C electrocatalyst was significantly higher than that using the PtNi/C catalysts. The current decay for the EOR was slower using PtSnNi/C compared to the one

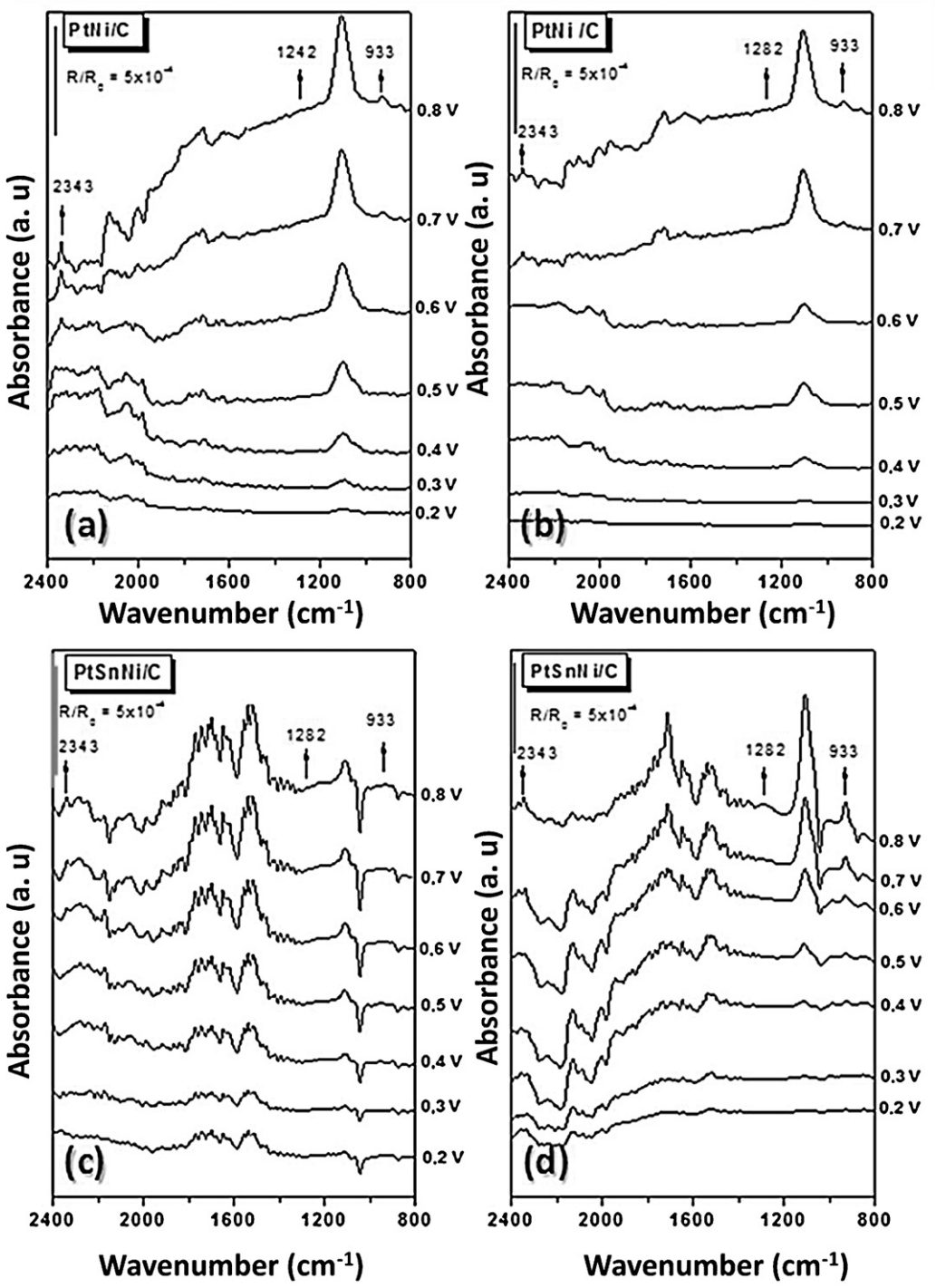

Fig. 8. The *in situ* FTIR spectra collected at several potentials for the ethanol oxidation reaction on PtNi/C (3:1) and PtSnNi/C (3:1:1) (a) and (c) before the accelerated stress tests; (b) and (d) after the accelerated stress tests. Backgrounds collected at 0.05 V (vs RHE).

for the same process using PtNi/C, which indicates less accumulation of adsorbed CO species. After the accelerated stress tests, the current densities decreased. A higher stability for the PtSnNi/C electrocatalysts was observed during the experimental time period.

At the end of the experimental time period, the current density (EOR) using PtSnNi/C (16 $mAmg_{Pt}^{-1}$) was considerably greater than that of the PtNi/C catalyst (0. 22 $mAmg_{Pt}^{-1}$). After the stress tests, the current obtained with the PtSnNi/C electrocatalyst at the end of the experimental period decreased by half. Even with a current decay, the electrocatalytic ethanol oxidation process is more effective with the PtSnNi/C electrocatalyst. The differences observed for the ethanol oxidation current densities measured before and after the stress tests are most likely due to the modification of the Sn and Ni oxyhydroxide species, which can contribute to a change in the pathways for the EOR. The effective number of electrons for the oxidation of ethanol is most likely higher when using the PtSnNi/C electrocatalyst than when using the PtNi/C electrocatalyst. Therefore, the current densities for the EOR are the highest for the PtSnNi/C electrocatalyst.

To study the EOR pathways before and after the stress tests, the products generated during this process were measured using "*in situ*" ATR-FTIR, and the results are shown in Fig. 8. It was possible to observe the adsorption bands related to acetaldehyde (933 cm^{-1}) [54], acetic acid (1282 cm^{-1}) [23] and CO_2 (2343 cm^{-1}) [55].

Using the PtNi/C electrocatalyst, the beginning of the acetaldehyde and CO_2 formation before (Fig. 8a) and after the stress tests was observed at 0.4 V and 0.6 V, respectively, which represents the primary production at high potentials. Therefore, the acetic acid band exhibited a low intensity. After the stress tests (Fig. 8b), the band related to CO_2 was observed at 0.7 V. Using the PtSnNi/C electrocatalysts, the formation of CO_2 occurred at 0.6 V (Fig. 8c), but after the stress tests, the production of acetaldehyde (from 0.3 V) and acetic acid (in smaller amounts) were greater than the production of CO_2 (Fig. 8d). To better evaluate the effect of the accelerated stress tests on the product formation from the ethanol oxidation reaction at different potentials (0.2 to 0.8 V), the integrated

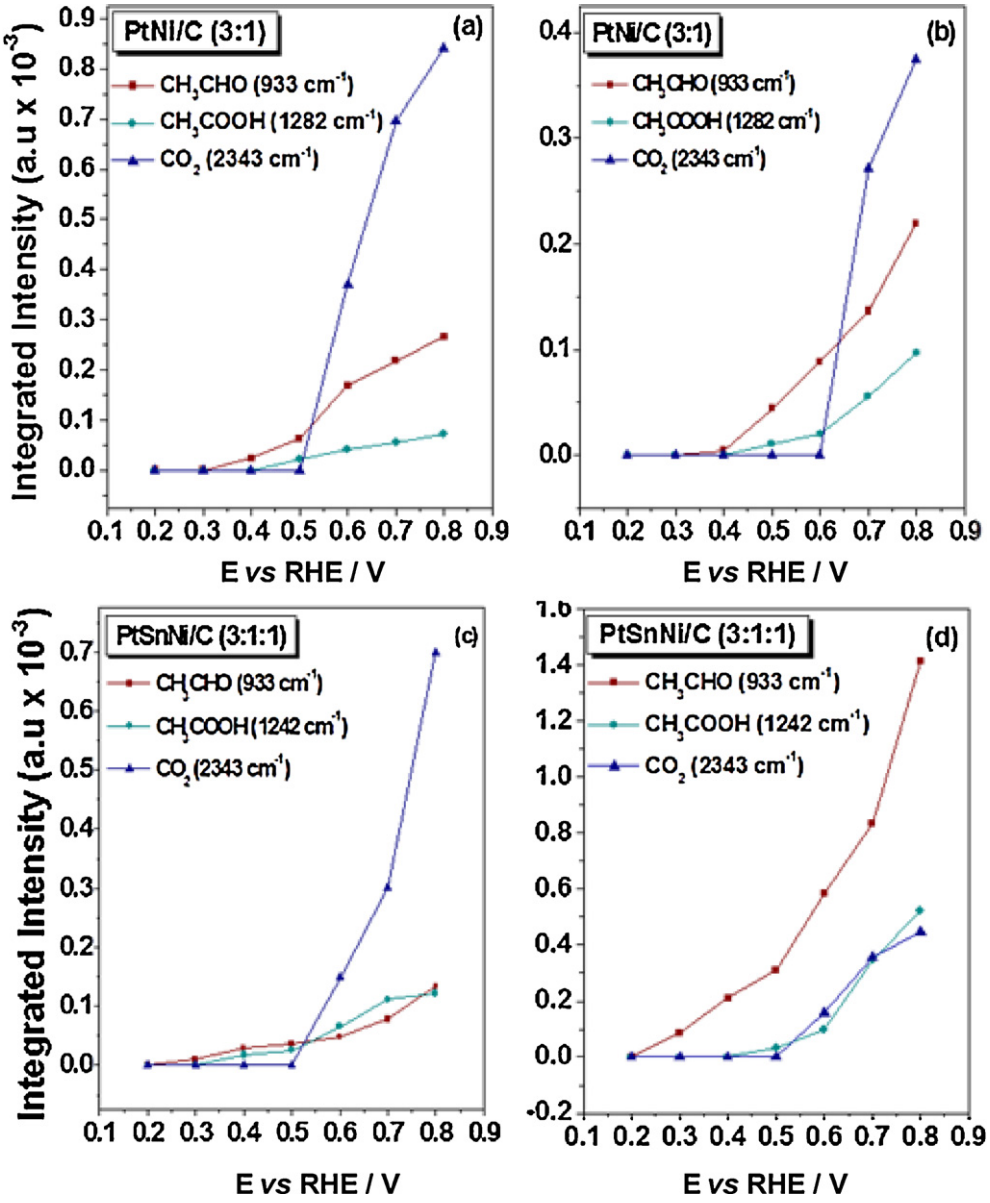

Fig. 9. Integrated CO_2, acetic acid (CH_3COOH) and acetaldehyde (CH_3CHO) band intensities as a function of the electrode potential for PtNi/C (3:1) and PtSnNi/C (3:1:1) (a) and (c) before the accelerated stress tests; (b) and (d) after the accelerated stress tests.

intensities of the acetaldehyde (CH_3CHO), acetic acid (CH_3COOH) and CO_2 bands are presented in Fig. 8.

For PtNi/C, the current density for the EOR, which was already low, exhibited a smaller decrease after the stress tests due to a slight increase in the ratio of acetaldehyde/acetic acid formation at 0.5 V (see Fig. 9a and b). In PtSnNi/C, the reduction in the current density after the stress tests was greater than that measured for the same reaction using PtNi/C because the acetaldehyde/acetic acid product ratio was higher for the prior case with fewer electrons involved in the process. Changes in the structure of the electrocatalysts may have occurred due the removal of the hydroxyl species, which causes the electrocatalyst to behave like pure Pt in which the ethanol oxidation reaction leads to the formation of acetaldehyde at low potentials. This result is in agreement with the results reported by Almeida et al. [31].

The low production of acetaldehyde and acetic acid with the PtNi/C electrocatalyst was observed until 0.5 V, and the generation of CO_2 occurred after 0.5 V. The activity of this electrocatalyst is most likely related to the bifunctional mechanism due to the presence of nickel oxide. However, there are two important aspects of the Ni effect combined with Pt: (i) the NiO/hydroxide species can cover the available Pt sites, which decreases the catalytic activity of PtNi/C, and (ii) the ability to enhance the oxidation of CO is less than that of PtSnNi/C, as shown in Fig. 5a and b.

Comparing the ATR-FTIR results for the EOR (Fig. 9), a greater amount of acetic acid is produced using PtSnNi/C compared to PtNi/C. This result can be explained by the presence of a PtSn alloy [15] where there are more available sites for the oxyhydroxide species in the presence of tin. In fact, a higher effective number of electrons is provided for the EOR using PtSnNi/C compared to PtNi/C, which explains the chronoamperometric behavior (see Fig. 8a and b).

For PtSnNi/C, the primary product measured by ATR-FTIR for the EOR is acetaldehyde before and after the accelerated stress tests. This behavior can be explained by the opposite effects of Ni and Sn in the electrocatalyst where there is filling of the d band levels of platinum due to Ni and shrinking of the d band levels of platinum due to Sn. The sum of these two effects are related to a condition similar to that observed on pure Pt (the presence of Sn and Ni also makes Pt retain their lattice parameters and their electrocatalytic activity is close to that of pure Pt). Therefore, the primary product is acetaldehyde. However, the presence of acetic acid before the stress tests is most likely associated with the bifunctional mechanism. After the stress tests, the amount of acetaldehyde produced is high. There are some possible reasons for this feature, including (i) Pt exposure and agglomeration during the cycling of Pt, (ii) reduction of oxyhydroxide species, (iii) loss of Ni and (iv) the effect of tin on Pt producing some small amount of acetic acid at higher intensity compared with the EOR with the same electrocatalyst before the stress tests.

For the ethanol oxidation reaction, Pt strongly adsorbs small organic molecules due to its electronic and structural characteristics. The addition of Sn expanded the Pt lattice parameter, which influences the adsorption of these organic molecules and the oxidation process. In addition, there is an electronic effect that decreases the d band center of Pt, weakening the adsorption of the intermediates as CO and releasing the active electrocatalytic sites. With the simultaneous addition of Ni, three possible effects were determined, as follows: (i) it is possible to obtain a lattice parameter size similar to that of pure Pt because there is a contraction of the Pt lattice parameters (opposite effect of tin), which slightly modifies the ethanol adsorption; (ii) the electronegativity difference in the metals (Sn and Ni) changes the electronic properties of Pt and weakens the adsorption of CO; and (iii) the possible formation of Ni and Sn metal oxides on the surface of the electrocatalyst may contribute to the oxidative removal of CO and formation of CO_2 via the bifunctional mechanism.

Thus, PtSnNi/C presented some good electrocatalytic properties for the oxidation of ethanol. The particles exhibited greater dispersion on the ternary electrocatalysts compared to the binary electrocatalyst, which increases the superficial area of the particles. The stability of Ni in the presence of tin is greater than without tin. The accelerated stress tests can change the structure of the electrocatalysts and the amount of Ni present. These tests can change the pathways for EOR, as shown in the *in situ* ATR-FTIR measurements.

4. Conclusions

In this work, we reported that the addition of Sn and Ni as auxiliary metals to Pt significantly improves the electrocatalytic activities for the ethanol oxidation reaction. The PtSnNi/C (3:1:1) nano-electrocatalyst exhibited greater activity than PtNi/C (3:1) with the presence of a lower onset potential and a higher peak current density for the EOR. Chronoamperometry tests indicated that the PtSnNi/C (3:1:1) catalysts have the highest current density and the lowest current density decay rate compared with both the PtSn/C (3:1) and PtNi/C (3:1) electrocatalysts. After the accelerated stress tests under repetitive potential cycling, the reaction activity for the oxidation of ethanol by the PtSnNi/C (3:1:1) nano-electrocatalyst remained higher than the cycled PtNi/C (3:1) catalyst.

The presence of Sn and Ni in the Pt-based electrocatalysts favors the formation of alloys and changes the electronic properties of the Pt, which weakens the adsorption of the intermediate products on the surface and improves the stability of the electrocatalyst. Therefore, the ternary alloy exhibited a lower dissolution of Ni than the binary alloy. Furthermore, the presence of Ni and Sn oxide/hydroxide species contribute to the increase in the electrocatalytic activity of the material and shifts the reaction pathway to the formation of acetaldehyde at low overpotentials and CO_2 at potentials greater than 0.5 V (for the PtNi/C electrocatalyst). However, for the PtSnNi/C electrocatalyst, the simultaneous presence of Sn and Ni retains the structural and electronic properties of the Pt-based electrocatalysts at values similar to that of pure Pt both before and after the stress tests, which primarily favors the formation of acetaldehyde and acetic acid (in lower amounts).

Acknowledgements

The authors wish to thank the Brazilian Funding Institutions CNPq, CAPES and FAPESP (2011/00008-2, 2010/16511-6, 2009/09145-6, 2010/03037-4), and UFABC for their financial and structural support. In addition, the authors wish to thank the Instituto Nacional de Ciência e Tecnologia (INCT) de Energia e Meio Ambiente (Process Number. 573.783/2008-0).

References

[1] D. Hotza, J.C.D. da Costa, Fuel cells development and hydrogen production from renewable resources in Brazil, International Journal Hydrogen of Energy 33 (2008) 4915.
[2] W.J. Zhou, B. Zhou, W.Z. Li, Z.H. Zhou, S.Q. Song, G.Q. Sun, Q. Xin, S. Douvartzides, M. Goula, P. Tsiakaras, Performance comparison of low-temperature direct alcohol fuel cells with different anode catalysts, Journal of Power Sources 126 (2004) 16.
[3] F.L.S. Purgato, S. Pronier, P. Olivi, A.R. de Andrade, J.M. Léger, G. Tremiliosi-Filho, K.B. Kokoh, Direct ethanol fuel cell: Electrochemical performance at 90 °C on Pt and PtSn/C electrocatalysts, Journal of Power Sources 15 (2012) 95.
[4] Z. Zhang, L. Xin, K. Sun, W. Li, Pd–Ni electrocatalysts for efficient ethanol oxidation reaction in alkaline electrolyte, International Journal of Hydrogen Energy 36 (2011) 12686.
[5] M. Ni, D.Y.C. Leung, M.K.H. Leung, A review on reforming bioethanol for hydrogen production, International Journal of Hydrogen Energy 32 (2007) 3238.

[6] J.A. Francesconi, M.C. Mussati, R.O. Mato, P.A. Aguirre, Analysis of the energy efficiency of an integrated ethanol processor for PEM fuel cell systems, Journal of Power Sources 167 (2007) 151.
[7] G. Tremiliosi-Filho, F.C. Simões, D.M. Anjos, F. Vigier, J.M. Léger, F. Hahn, C. Coutanceau, E.R. González, A.R. Andrade, P. Olivi, K.B. Kokoh, Electroactivity of tin modified platinum electrodes for ethanol electrooxidation, Journal of Power Sources 167 (1) (2007) 1.
[8] W.J. Zhou, S.Q. Song, W.Z. Li, Z.H. Zhou, G.Q. Sun, Q. Xin, S. Douvartzides, P. Tsiakaras, Direct ethanol fuel cells based on PtSn anodes: the effect of Sn content on the fuel cell performance, Journal of Power Sources 140 (2005) 50.
[9] X. Xue, J. Ge, T. Tian, C. Liu, W. Xing, T. Lu, Enhancement of the electrooxidation of ethanol on Pt–Sn–P/C catalysts prepared by chemical deposition process, Journal Power Sources 172 (2007) 560.
[10] S.Q. Song, W.J. Zhou, Z.H. Zhou, L.H. Jiang, G.Q. Sun, Q. Xin, V. Leontidis, S. Kontou, P. Tsiakaras, Direct ethanol PEM fuel cells: The case of platinum based anodes, International Journal of Hydrogen Energy 30 (2005) 995.
[11] F. Vigier, C. Coutanceau, F. Hahn, E.M. Belgsir, C. Lamy, On the mechanism of ethanol electro-oxidation on Pt and PtSn catalysts: electrochemical and in situ IR reflectance spectroscopy studies, Journal of Electroanalytical Chemistry 563 (2004) 81.
[12] E.V. Spinacé, L.A.I. do Vale, R.R. Dias, A.O. Neto, M. Linardi, PtSn/C electrocatalysts prepared by different methods for direct ethanol fuel cell, Studies in Surface Science and Catalysis 162 (2006) 617.
[13] L. Jiang, H. Zang, G. Sun, Q. Xin, Influence of preparation method on the performance of PtSn/C anode electrocatalyst for direct ethanol fuel cells, Chinese Journal of Catalysis 27 (1) (2006) 15.
[14] T.S. Almeida, L.M. Palma, P.H. Leonello, C. Morais, K.B. Kokoh, A.R. De Andrade, An optimization study of PtSn/C catalysts applied to direct ethanol fuel cell: Effect of the preparation method on the electrocatalytic activity of the catalysts, Journal of Power Sources 215 (2012) 53.
[15] J.C.M. Silva, L.S. Parreira, R.F.B. De Souza, M.L. Calegaro, E.V. Spinacé, A.O. Neto, M.C. Santos, PtSn/C alloyed and non-alloyed materials: Differences in the ethanol electro-oxidation reaction pathways, Applied Catalysis B: Environmental 110 (2) (2011) 141.
[16] M. Zhu, G. Sun, Q. Xin, Effect of alloying degree in PtSn catalyst on the catalytic behavior for ethanol electro-oxidation, Electrochimica Acta 54 (2009) 1511.
[17] D.F. Silva, A.N. Geraldes, A.O. Neto, E.S. Pino, M. Linardi, E.V. Spinacé, W.A.A. Macedo, J.D. Ardisson, Preparation of $PtSnO_2$/C electrocatalysts using electron beam irradiation, Materials Science and Engineering B 175 (2010) 261.
[18] F.H.B. Lima, E.R. Gonzalez, Ethanol electro-oxidation on carbon-supported Pt–Ru, Pt–Rh and Pt–Ru–Rh nanoparticles, Electrochimica Acta 53 (2008) 2963.
[19] Y.Y. Tong, H.S. Kim, P.K. Babu, P. Waszczuk, A. Wieckowski, E. Oldfield, An NMR investigation of CO tolerance in a Pt/Ru fuel cell catalyst, Journal of the American Chemical Society 124 (2002) 468.
[20] S. Alayoglu, A.U. Nilekar, M. Mavrikakis, B. Eichhorn, Ru-Pt core-shell nanoparticles for preferential oxidation of carbon monoxide in hydrogen, Nature Materials 7 (2008) 333.
[21] Z. Mingyuan, S. Gongquan, L. Huanqiao, C. Lei, X. Qin, Effect of the Sn(II)/Sn(IV) redox couple on the activity of PtSn/C for ethanol electro-oxidation, Chinese Journal of Catalysis 29 (8) (2008) 765.
[22] J.H. Kim, S.M. Choi, S.H. Nam, M.H. Seo, S.H. Choi, W.B. Kim, Influence of Sn content on PtSn/C catalysts for electrooxidation of C1–C3 alcohols: Synthesis, characterization, and electrocatalytic activity, Applied Catalysis B: Environmental 82 (2008) 89.
[23] R.F.B. De Souza, L.S. Parreira, D.C. Rascio, J.C.M. Silva, E. Teixeira-Neto, M.L. Calegaro, E.V. Spinace, A.O. Neto, M.C. Santos, Study of ethanol electro-oxidation in acid environment on Pt3Sn/C anode catalysts prepared by a modified polymeric precursor method under controlled synthesis conditions, Journal of Power Sources 195 (2010) 1589.
[24] L. Jiang, Z. Zhou, W. Li, W. Zhou, S. Song, H. Li, G. Sun, Q. Xin, Effects of treatment in different atmosphere on Pt3Sn/C electrocatalysts for ethanol electro-oxidation, Energy Fuels 18 (2004) 866.
[25] J. Bagchi, S.K. Bhattacharya, The effect of composition of Ni-supported Pt-Ru binary anode catalysts on ethanol oxidation for fuel cells, Journal of Power Sources 163 (2) (2007) 661.
[26] G.W. Huber, J.W. Shabaker, J.A. Dumesic, Raney Ni-Sn catalyst for H_2 production from biomass-derived hydrocarbons, Science 300 (2003) 2075.
[27] H. Yang, J. Zhang, S. Kumar, H. Zhang, R. Yang, J. Fang, S. Zou, Monodisperse and highly active PtNi nanoparticles for O_2 reduction, Electrochemistry Communications 11 (2009) 2278.
[28] C.-W. Liu, Y.-W. Chang, Y.-C. Wei, K.-W. Wang, The effect of oxygen containing species on the catalytic activity of ethanol oxidation for PtRuSn/C catalysts, Electrochimica Acta 56 (5) (2011) 2574.
[29] R.F.B. De Souza, L.S. Parreira, J.C.M. Silva, F.C. Simões, M.L. Calegaro, M.J. Giz, G.A. Camara, A.O. Neto, M.C. Santos, PtSnCe/C electrocatalysts for ethanol oxidation: DEFC and FTIR "in-situ" studies, International Journal of Hydrogen Energy 36 (18) (2011) 11519.
[30] J. Tayal, B. Rawat, S. Basu, Bi-metallic and tri-metallic Pt–Sn/C, Pt–Ir/C, Pt–Ir–Sn/C catalysts for electro-oxidation of ethanol in direct ethanol fuel cell, International Journal of Hydrogen Energy 36 (22) (2011) 14884.
[31] T.S. Almeida, K.B. Kokoh, A.R. De Andrade, Effect of Ni on Pt/C and PtSn/C prepared by the Pechini method, International Journal of Hydrogen Energy 36 (2011) 3803.
[32] A. Bonesi, G. Garaventa, W.E. Triaca, A.M. Castro Luna, Synthesis and characterization of new electrocatalysts for ethanol oxidation, International Journal of Hydrogen Energy 33 (2008) 3499.
[33] E. Ribadeneira, B.A. Hoyos, Evaluation of Pt–Ru–Ni and Pt–Sn–Ni catalysts as anodes in direct ethanol fuel cells, Journal of Power Sources 180 (2008) 238.
[34] S. Zhang, X.-Z. Yuan, J.N.C. Hin, H. Wang, K.A. Friedrich, M. Schulze, A review of platinum-based catalyst layer degradation in proton exchange membrane fuel cells, Journal of Power Sources 194 (2009) 588.
[35] S.C. Zignani, E. Antolini, E.R. Gonzalez, Stability of Pt–Ni/C (1:1) and Pt/C electrocatalysts as cathode materials for polymer electrolyte fuel cells: Effect of ageing tests, Journal of Power Sources 191 (2009) 344.
[36] S. Garcia, R. Galbeiro, S.G. Silva, C.S. Nomura, F.R.P. Rocha, I. Gaubeur, An environmentally friendly analytical procedure for nickel determination by atomic and molecular spectrometry after cloud point extraction in different samples, Analytical Methods 4 (2012) 2429.
[37] N.M. Deraz, Effect of NiO content on structural, surface and catalytic characteristics of nano-crystalline NiO/CeO_2 system, Ceramics International 38 (1) (2012) 747.
[38] K.-W. Park, J.-H. Choi, B.-K. Kwon, S.-A. Lee, H.-Y. Ha, S.-A. Hong, Y.-E. Sung, H. Kim, A. Wieckowski, Chemical and electronic effects of Ni in Pt/Ni and Pt/Ru/Ni alloy nanoparticles in methanol electrooxidation, Journal of Physical Chemistry B 106 (2002) 1869.
[39] P.S. Correa, E.L. da Silva, R.F. da Silva, C. Radtke, B. Moreno, E. Chinarro, C.F. Malfatti, Effect of decreasing platinum amount in Pt–Sn–Ni alloys supported on carbon as electrocatalysts for ethanol electrooxidation, International Journal of Hydrogen Energy 37 (2012) 9314.
[40] E.V. Spinacé, M. Linardi, A.O. Neto, Co-catalytic effect of nickel in the electro-oxidation of ethanol on binary Pt–Sn electrocatalysts, Electrochemistry Communications 7 (2005) 365.
[41] J.M. Sieben, M.E. Duarte, Nanostructured Pt and Pt–Sn catalysts supported on oxidized carbon nanotubes for ethanol and ethylene glycol electro-oxidation, International Journal of Hydrogen Energy 36 (2011) 3313.
[42] E.M. Cunha, J. Ribeiro, K.B. Kokoh, A.R. de Andrade, Preparation, characterization and application of Pt–Ru–Sn/C trimetallic electrocatalysts for ethanol oxidation in direct fuel cell, International Journal of Hydrogen Energy 36 (17) (2011) 11034.
[43] G. Wang, Y. Gao, Z. Wang, C. Du, J. Wang, G. Yin, Investigation of PtNi/C anode electrocatalysts for direct borohydride fuel cell, Journal of Power Sources 195 (2010) 185.
[44] M.V. Martínez-Huerta, S. Rojas, J.L. Gómez de la Fuente, P. Terreros, M.A. Peña, J.L.G. Fierro, Effect of Ni addition over PtRu/C based electrocatalysts for fuel cell applications, Applied Catalysis B: Environmental 69 (1/2) (2006) 75.
[45] Y.H. Cho, T.Y. Jeon, J.W. Lim, Y.H. Cho M.A., N. Jung, S.J. Yoo, W.S. Yoon, Y.E. Sung, Performance and stability characteristics of MEAs with carbon-supported Pt and Pt1Ni1 nanoparticles as cathode catalysts in PEM fuel cell, International Journal of Hydrogen Energy 36 (2011) 4394.
[46] S. Lee, H.J. Kimb, S.M. Choib, M.H. Seob, W.B. Kim, The promotional effect of Ni on bimetallic PtNi/C catalysts for glycerol electrooxidation, Applied Catalysis A: General 429–430 (2012) 39.
[47] J.W. Shabaker, G.W. Huber, J.A. Dumesic, Aqueous-phase reforming of oxygenated hydrocarbons over Sn-modified Ni catalysts, Journal of Catalysis 222 (2004) 180.
[48] D.B. Kim, H.-J. Chun, Y.K. Lee, H.-H. Kwon, H.-I. Lee, Preparation of Pt/NiO-C electrocatalyst and heat-treatment effect on its electrocatalytic performance for methanol oxidation, International Journal of Hydrogen Energy 35 (2010) 313.
[49] A. Belanger, A.K. Vijh, The hydrogen evolution reaction on Ni-Sn alloys and intermetallics, Surface and Coatings Technology 28 (1986) 93.
[50] T.J. Tiainent, R.B. Schwarz, Synthesis and characterization of mechanically alloyed Ni-Sn powders, Journal of the Less-Common Metals 140 (1988) 99.
[51] F. Colmati, E. Antolini, E.R. Gonzalez, Ethanol oxidation on carbon supported Pt-Sn electrocatalysts prepared by reduction with formic acid, Journal of the Electrochemical Society 154 (2007) B39.
[52] M. Arenz, V. Stamenkovic, B.B. Blizanac, K.J.J. Mayrhofer, N.M. Markovic, P.N. Ross, Carbon-supported Pt-Sn electrocatalysts for the anodic oxidation of H2, CO, and H2/CO mixtures. Part II: The structure-activity relationship, Journal of Catalysis 232 (2) (2005) 402.
[53] T. Sato, K. Kunimatsu, H. Uchida, M. Watanabe, Adsorption/oxidation of CO on highly dispersed Pt catalyst studied by combined electrochemical and ATR-FTIRAS methods Part 1. ATR-FTIRAS spectra of CO adsorbed on highly dispersed Pt catalyst on carbon black and carbon un-supported Pt black, Electrochimica Acta 534 (3) (2007) 1265.
[54] M. Li, A. Kowal, K. Sasaki, N. Marinkovic, D. Su, E. Korach, P. Liu, R.R. Adzic, Ethanol oxidation on the ternary Pt-Rh-SnO_2/C electrocatalysts with varied Pt:Rh:Sn ratios, Electrochimica Acta 55 (2010) 4331.
[55] G.A. Camara, T. Iwasita, Parallel Pathways of methanol Oxidation: The effect of ethanol concentration, Journal Electroanalytical Chemistry 578 (2005) 315.